Hindawi
Advances in Materials Science and Engineering
Volume 2019, Article ID 7029671, 11 pages
https://doi.org/10.1155/2019/7029671

Research Article

Actual Temperature Evolution of Thick Raft Concrete Foundations and Cracking Risk Analysis

Yuwen Ju and Honggang Lei

School of Architecture and Civil Engineering, Taiyuan University of Technology, Taiyuan 030024, China

Correspondence should be addressed to Yuwen Ju; juyuwen@tyut.edu.cn and Honggang Lei; lhgang168@126.com

Received 30 October 2018; Accepted 2 January 2019; Published 21 January 2019

Academic Editor: Paolo Andrea Carraro

Heat of the hydration-induced temperature evolution of a 3.30 m thick raft concrete foundation for wind turbines at the early ages was monitored in situ through a temperature sensor testing system. The temperature variation patterns and risk of cracking were studied. Finite element analysis (FEA) conducted on the temperature fields determined the lower thickness threshold requiring temperature control. A comprehensive temperature control approach suitable for thick raft foundations was proposed based on a practical engineering project. Temperature monitoring and analysis results showed that the early temperature field evolution featured two characteristic phases: heat accumulation and heat release. A remarkable temperature gradient was observed along the vertical direction of the foundation. The maximum temperature difference between the concrete core and the top surface was approximately 35°C, indicating a risk of cracking. The accuracy of the FEA was ensured by adopting the concrete heat generation rate obtained from the adiabatic temperature rise test. A further FEA performed on foundations with various thicknesses demonstrated that a thicker foundation corresponded to a higher vertical temperature gradient. Moreover, a raft thickness larger than 2.50 m corresponded to a maximum temperature difference between the concrete core and the surface higher than 25°C, above which cracking prevention measures should be taken. Field test results proved the applicability of a suite of temperature feedback regulation measures proposed herein, including layered pouring, thermal insulation, and in situ real-time temperature monitoring, to thick raft mass concrete structures with relatively small volumes. Good control of temperature difference was achieved using this approach.

1. Introduction

The concept of mass concrete stems from water resource projects. Initially, it mostly referred to concrete used for dams, such as the Arrowrock Dam in the US that opened in 1915, the Hoover Dam in the US that opened in 1933, the Toktogul hydropower station in the former Soviet Union that opened in 1977, and the world-renowned Three Gorges Dam in China that opened in 1994 [1–4]. These dams are classified as mass concrete structures. The construction of mass concrete structures often faces a key technical challenge, i.e., the control of temperature cracking. From the standpoint of internal stress, a sufficiently large thermal stress would lead to cracks, which are referred to as temperature cracks, when the temperature difference between the inside and the surface of concrete exceeds a threshold. This topic has been extensively studied [5–12].

With the rapid social and economic development, large-sized, high-volume, and poured concrete structures have been increasingly used in sectors other than water resource projects. Thick raft concrete foundations for high-rise buildings, concrete diaphragm wall for subway tunnels, and thick raft concrete foundations for power generation facilities have been widely employed particularly in industrial and civil engineering. For instance, the foundation rafts of the Jin Mao Tower in Shanghai and the new office building of CCTV in Beijing are as thick as 5 m and 7 m, respectively. Although these raft foundation structures are smaller than dams in size, a relatively large temperature difference between the inside and the concrete surface can still be observed because of their remarkable thickness. Such temperature difference results in temperature cracks, which hinders the normal use of the structure. Engineering practices have shown a noticeable increase in the probability

of temperature cracking occurrence when the temperature difference is roughly larger than 25°C [13]. A previous study reported that temperature cracking happens to a concrete structure during construction because of the thermal stress formed when the concrete surface temperature dipped to 9°C after a sudden strike of cold wave, while the internal temperature remains at 32°C [14]. According to Reference [15], with a minimum cross-section side of over 80 cm, a concrete structure with an expected temperature difference between the core and the ambient environment of over 25°C is referred to as a mass concrete structure, on which temperature cracking control should be implemented [15]. Therefore, the concept of mass concrete has been expanded to structures with large temperature gradients, whose size, however, might not be comparable to traditional dams. The aforementioned smaller-volume thick raft foundations also fall into this category.

Massive water resource constructions, such as dams, have been extensively probed in the field of concrete engineering. In contrast, only a few studies in the literature have reported on the thick raft mass concrete foundation structures used in general industrial and civil constructions, which are of course significantly smaller in size [16]. This type of concrete structures features the use of modern cement in large quantities and the continuous improvement in manufacturing techniques with distinctively complex temperature-field characteristics caused by the heat of hydration during the early ages after pouring. Currently, the common practice in the construction of thick raft concrete foundations is to roughly estimate the heat release and temperature rise using empirical methods, based on which a decision is then made pertaining to whether temperature control measures should be taken. These methods are not able to accurately reflect the actual temperature fields of the concrete [17]; hence, the corresponding temperature cracking prevention measures are primitive and blind to specific situations. Therefore, studying the temporal and spatial variation patterns of the actual temperature field at the early ages and investigating the associated cracking risks are theoretically and practically important in effectively avoiding temperature cracking of the thick raft concrete foundations during construction.

Based on a practical engineering project, this study obtained the real-time temperature monitoring data within 18 days after concrete pouring by arranging temperature sensors in a thick raft foundation for a wind turbine. The temperature variation patterns were observed by analyzing the test data. The concrete cracking risks were also discussed. A finite element analysis (FEA) was performed on the temperature fields of foundations with various levels of raft thickness, from which a thickness threshold requiring temperature control was determined. Finally, effective temperature control measures for thick raft foundations were proposed for practical engineering applications.

2. Materials and Methods

2.1. Engineering Background. The engineering background of this study was a wind turbine foundation project in North China, which had 21 identical wind turbines supported by thick raft concrete foundation structures that were also identical. Among them, Foundation 1, without any temperature control, was used for the temperature field test, whereas foundations 2–21 had temperature control measures based on the temperature test results obtained from Foundation 1. The foundation was 18 m in both length and width and has a thickness of 3.3 m. Its upper part was a cylinder with a 7 m diameter. The concrete had a C35 grade, whose mixing ratio is shown in Table 1. Foundation 1 was poured within a 24 h period using the continuous layered pouring method. Figure 1 are photos of Foundation 1 before and after pouring.

2.2. Design of the Field Test. Before pouring, multiple sensors were set inside Foundation 1 to monitor the temperature variations. They were installed at different vertical positions of the foundation, as shown in Figure 2. In addition, two ambient temperature monitoring points were set outside the foundation to provide temperature boundary conditions for the FEA model. Figure 3 illustrates the sensor installation layout before pouring.

2.3. Design of the Adiabatic Temperature Rise Test. The adiabatic temperature rise test aims at obtaining the temperature evolution inside the concrete specimens under adiabatic conditions, where the value of temperature rise measures the heat released from the hydration reaction of the cementing material of the concrete [18]. In the current seven-day test, cylinder specimens (40 cm in both diameter and height) were made from materials with the same mixing ratio used in a real construction (Table 1). A series of adiabatic temperature rises versus equivalent age curves were obtained. The test results provided benchmark data for calculating the heat generation rate of concrete in the subsequent FEA.

3. Results and Analysis

3.1. Temperature Monitoring Results and Analysis

3.1.1. Temporal Variations of the Temperature Field. The temperatures at various sensor installation points of Foundation 1 within 18 days after pouring were recorded through in situ real-time monitoring. Figures 4–6 show the temperature-time curves of different sensors, from which a similar pattern was observed. That is, the temperatures at all monitoring points inside the foundation rapidly increased after pouring. They then slowly decayed after peaking until a relatively steady state was reached. Based on these curves, the temperature evolution of the concrete foundation can be approximately divided into two following phases with distinct characteristics:

(1) Heat accumulation phase (i.e., temperature rise phase): this phase primarily featured heat build-up and temperature increase. A considerable amount of heat was generated because of the hydration reaction occurring in a large volume of concrete. The rate of

Table 1: Concrete mixing ratio (unit: kg).

Cement	Fly ash	Aggregate	Sand	Water	Admixture
385.0	68.0	106.5	725.0	179.0	10.4

(a)

(b)

Figure 1: Photos of Foundation 1. (a) Before pouring. (b) After demolding.

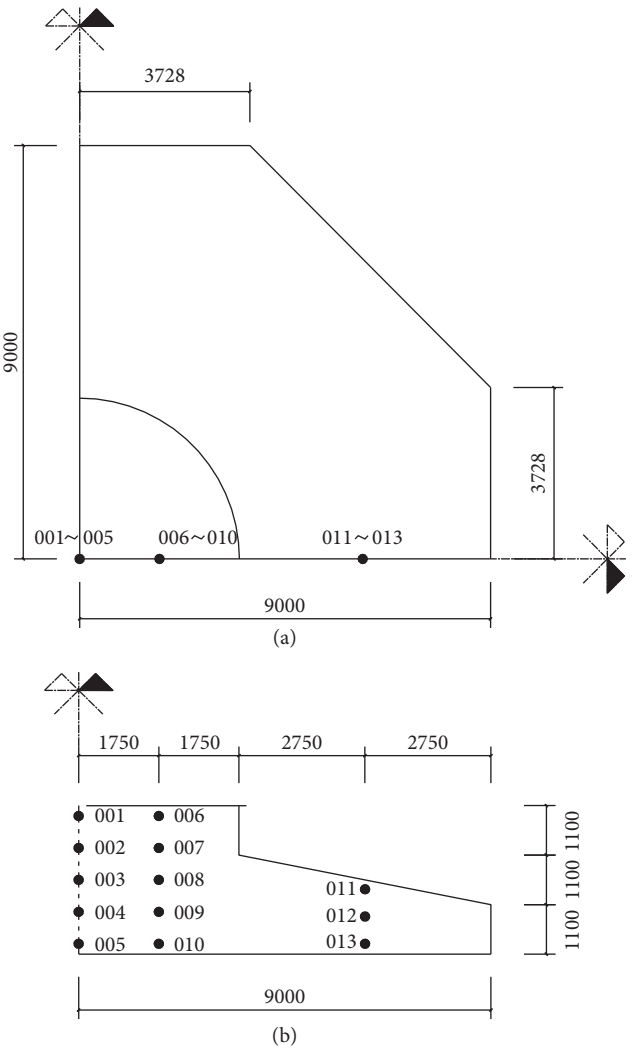

Figure 2: Layout of the temperature sensors: (a) top view and (b) side view.

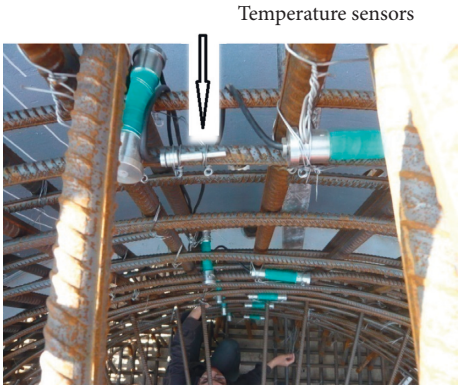

Figure 3: In situ installation of the temperature sensors.

heat generation inside the foundation was higher than the rate of heat dissipation from the foundation surface. Consequently, heat continuously built up within the foundation, leading to the rising and peaking of temperature at all monitoring points. Figures 4–6 also illustrate that, although temperature rise showed a similar pattern across the foundation, the temperature peak values and the ages at which peaks occurred varied. For example, the maximum peak (approximately 73°C) occurred at Point 003, which was at the foundation core, roughly 4 days after pouring; Point 002, which was close to the foundation surface, had a temperature peak of 67°C 3 days after pouring. These results suggested that the heat accumulation phase lasted longer at locations closer to the foundation core, leading to higher temperature peaks. During this phase, the average temperature rise rate across the foundation was 18°C per day.

(2) Heat release phase (i.e., temperature decay phase): this phase primarily featured heat conduction and dissipation. That is, heat generated from hydration transferred to the ambient environment and the neighboring earth, leading to the slow decline of the foundation's temperature. After heat transfer from the concrete, the temperature curves of the neighboring earth showed different fluctuation levels. A more intense fluctuation was observed at locations closer to the foundation surface. For example, Figure 4 shows that the 002 curve only exhibited a slight fluctuation during temperature decay, whereas the

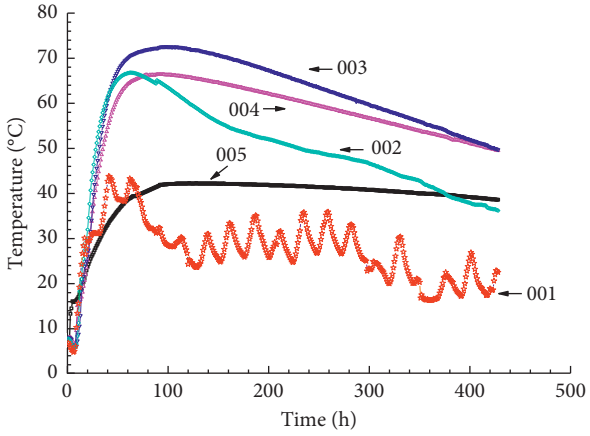

Figure 4: Measured temperature evolution of Points 001–005.

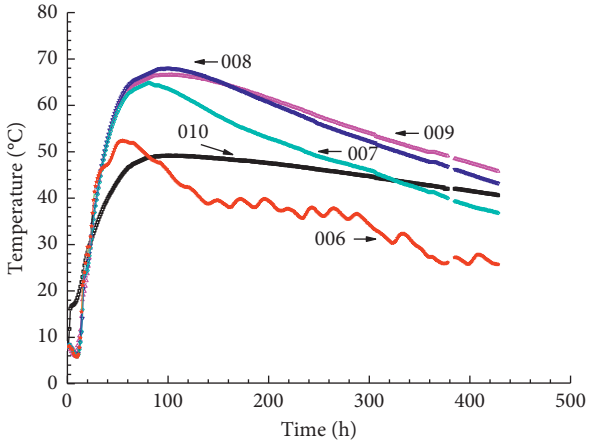

Figure 5: Measured temperature evolution of Points 006–010.

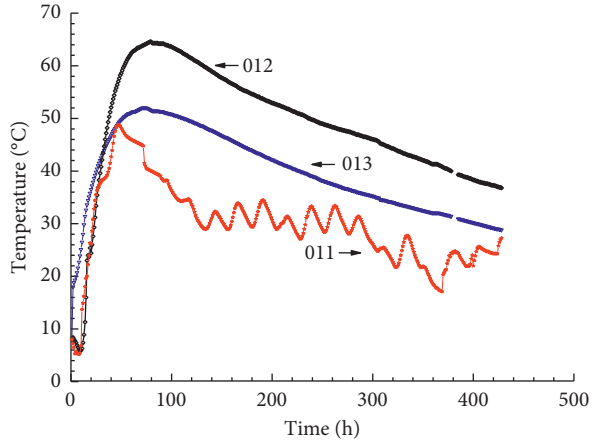

Figure 6: Measured temperature evolution of Points 011–013.

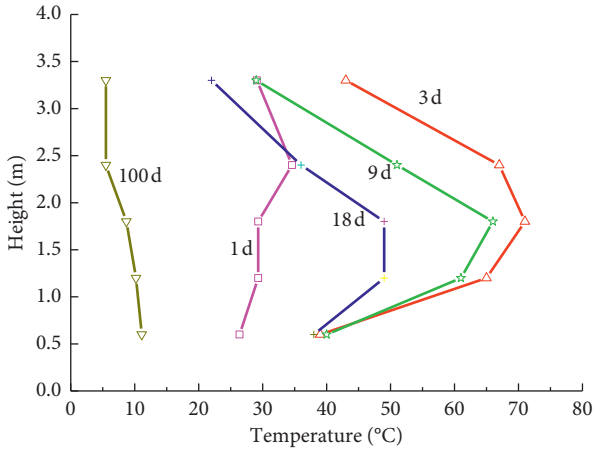

Figure 7: Temperature variation along the vertical direction of the foundation.

001 curve had remarkably more fluctuations because of the impact of the ambient temperature. The average temperature decay rate across the foundation during this phase was 1°C per day.

The temperature evolution of the foundation top and bottom was different from that of the internal locations. The sensor at the top had the lowest temperature peak (approximately 44°C), becoming sinusoidal after roughly 50 h, followed by a sharp decline. This was caused by the top being more susceptible to the environmental impact, thereby having a higher heat release rate compared to other locations. In contrast, the temperature at the foundation bottom declined in a slow fashion after peaking because the earth below the foundation had a relatively low heat conductivity, where heat dissipation was slower than heat accumulation.

3.1.2. Temperature Variation along the Vertical Direction of the Foundation. Temperature gradient is one of the main reasons leading to the cracking of mass concrete structures [9]. Therefore, the temperature gradient of the concrete must be fully considered when analyzing the reasons leading to the cracking of mass concrete. Figure 7 shows the temperature variation along the vertical direction of the foundation at different ages. Evident temperature gradients existed in the vertical direction. The maximum gradient occurred at an age of 9 days, with the temperature difference between the foundation core and the top being 35°C. At a sufficiently late age, the temperatures at different heights approached the ambient temperature after the heat of the foundation was gradually released.

3.1.3. Temperature Variation along the Horizontal Direction of the Foundation. Figures 8 and 9 show the temperature evolution of two pairs of sensors (i.e., 002/007 and 004/009, respectively) at two different heights of the foundation. The two curves in each figure were very similar; hence, the temperature of different locations of the same height can be thought as approximately equal (i.e., zero temperature gradient along the horizontal direction of the foundation) when the foundation thickness was significantly smaller than the other two dimensions.

3.1.4. Cracking Risk Analysis of the Thick Raft Concrete Foundation. Based on the actual temperature evolution of

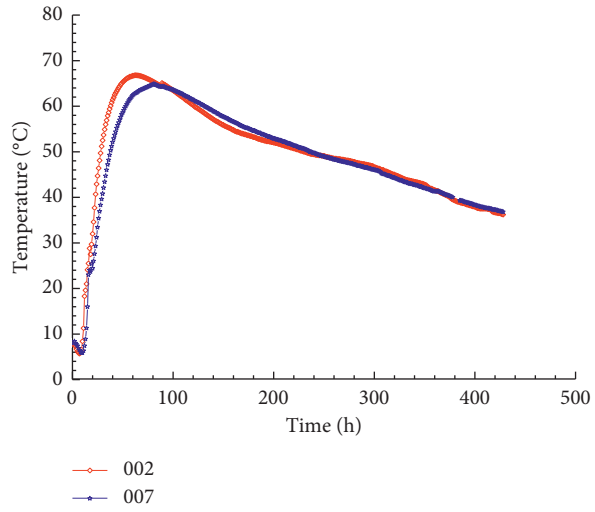

Figure 8: Temperature comparison between Points 002 and 007.

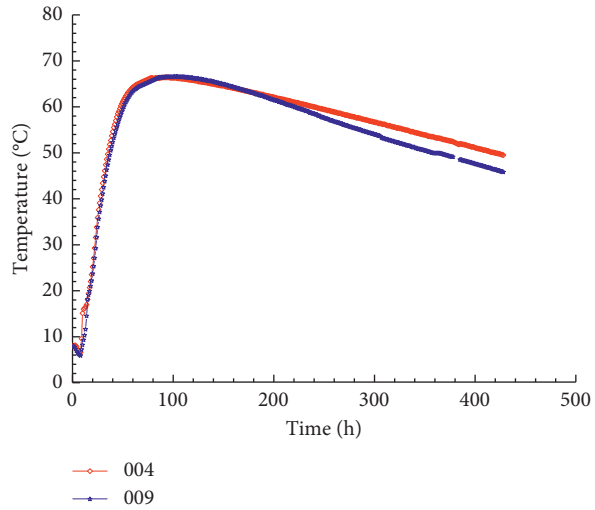

Figure 9: Temperature comparison between Points 004 and 009.

Foundation 1 discussed earlier, the cracking risk of the thick raft concrete foundation can be analyzed from the perspective of the two identified phases:

(1) Temperature rise phase: according to the spatial variation of temperature, the internal part of the concrete was the high-temperature zone, whereas the part close to the foundation surface was the low-temperature zone. The high-temperature zone was dominated by compressive stress because of the difference in temperature rise, whereas the low-temperature zone was dominated by tensile stress. However, the elastic modulus at the early ages was small; hence, the compressive and tensile stress values in this phase were quite small.

(2) Temperature decay phase: the elastic modulus of the concrete gradually increased to as large as 90% of the eventual value [14]. Moreover, as discussed earlier, the maximum temperature difference between the core and the surface was 35°C because of the large temperature gradient existing between the foundation core and surface. Hence, the core had a higher magnitude of temperature decay compared to the surface; thus, tensile stress was generated because the region with a stronger temperature decay was constrained during contraction by the region with a weak temperature decay. A significantly larger value of tensile stress was observed in this phase because of the increasing elastic modulus.

As a result, the compressive stress inside the concrete, which was generated during the temperature rise phase, was counteracted by the tensile stress generated during the temperature decay phase. The eventual combined effect was the creation of a tensile stress field with fairly large values inside the concrete while the surface was turned into a compressive stress field. A larger temperature gradient between the core and the surface led to a higher tensile stress inside the foundation, making it more likely to reach the ultimate tensile stress of the concrete and the crack. Previous studies have shown that concrete is highly susceptible to cracking when the temperature difference between the core and the surface is higher than 25°C [14, 19]. The temperature difference measured in the current study was 35°C, which is significantly higher than the previously reported threshold and indicated the risk of cracking. Therefore, temperature control measures should be taken to prevent the crack occurrence at the early ages.

3.2. FEA of the Temperature Field. The finite element method was used in our simulation to further investigate the temperature variation patterns under different raft thicknesses. The precision of the temperature FEA mostly depends on the input values of the thermal properties of concrete, among which the heat generation rate is of paramount significance [20].

3.2.1. Calculation of the Concrete Heat Generation Rate Based on the Adiabatic Temperature Rise Test. Based on the principle of heat balance, the heat conductivity equation for the heat of hydration of concrete is [9, 21]

$$\frac{\partial T}{\partial t} = \alpha\left(\frac{\partial^2 T}{\partial x^2} + \frac{\partial^2 T}{\partial y^2}\frac{\partial^2 T}{\partial z^2}\right) + \frac{Q(t)}{c\rho} \quad \forall (x, y, z) \in R, \qquad (1)$$

where T is the temperature in °C; t is the physical time in h; a is the thermal conductivity of concrete in kJ/(m·h·°C); $Q(t)$ is the heat generation rate of concrete in kJ/m^3·h; c is the specific heat of concrete in kJ/(kg·°C); and ρ is the density of concrete in kg/m^3.

The key to the current FEA is the determination of the heat generation rate of concrete, $Q(t)$, because it is not only dependent on the material properties of the concrete (primarily the mixing ratio) but also affected by the temporal history of the concrete temperature. Based on this consideration, the adiabatic temperature rise test is undoubtedly the most accurate method to determine this quantity. Figure 10 shows the adiabatic temperature of the concrete versus the equivalent age t_e obtained from the test.

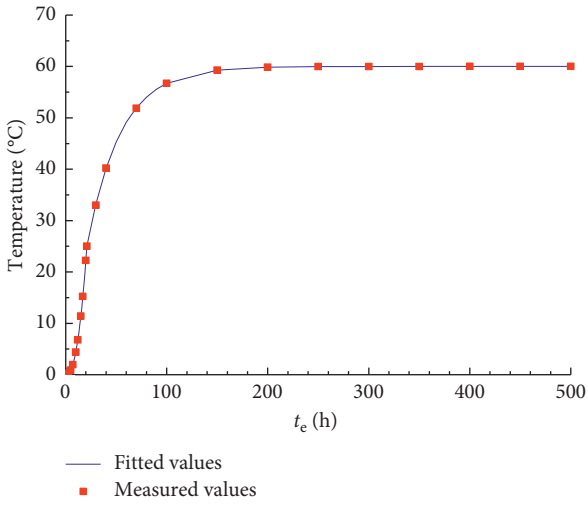

Figure 10: Adiabatic temperature rise test curve.

t_e, which is defined by equation (3), is associated with the temporal history of the concrete temperature.

The measured temperature values shown in Figure 10 can be fitted by the following equation [22]:

$$\theta(t_e) = \begin{cases} 0.02t_e^{2.342}, & t_e \le 21 \text{ h}, \\ 60 - 35\ \exp[-0.03(t_e - 21)], & t_e \ge 21 \text{ h}, \end{cases} \quad (2)$$

where θ is the value of adiabatic temperature rise in °C and t_e is the equivalent age defined as follows [19]:

$$t_e = \int_0^t \exp\left[\frac{E_h}{R}\left(\frac{1}{T_0} - \frac{1}{T(t)}\right)\right] dt, \quad (3)$$

where E_h is the activation energy of the hydration reaction in kJ/mol; R is the ideal gas constant in J/mol/K; and T_0 and T are the reference temperature and the actual temperature history of the concrete in K, respectively. In the current analysis, $E_h/R = 2400$ K and $T_0 = 293.15$ K.

Under adiabatic conditions, equation (1) can be written as follows:

$$\frac{\partial \theta}{\partial t} = \frac{Q(t)}{c\rho}. \quad (4)$$

Based on equations (2)–(4), $Q(t)$ can be obtained by calculating the derivative of θ with respect to age (time). It was then used in the ANSYS model to perform a transient analysis of the temperature field.

3.2.2. Comparison between the FEA Calculated Data and the In Situ Measured Data for Foundation 1. An FEA simulation was performed on the temperature field of Foundation 1 after pouring. Construction and solving of the computational model were both conducted in FEA software, ANSYS. According to geometric symmetry, 1/4 of the model consisting of concrete and earth was computed. Figure 11 depicts the concrete meshing. The main thermal parameters were determined by referring to relevant experiments and literature [23], as shown in Table 2.

The calculated temperature evolution of some representative monitoring points shown in Figure 2 is plotted in Figures 12–14. The calculated and measured temperature curves matched well, except for the monitoring points near the concrete surface. This result suggested that the method used for calculating the heat generation rate, the construction of the finite element model, and the determination of relevant thermal parameters were all valid. Note that the ambient temperature dramatically fluctuated with the weather conditions, making it hard to accurately set the temperature boundary conditions in the FEA. This was the main factor responsible for the discrepancy between the calculated and measured values near the concrete surface.

In practical construction, different mixing ratios correspond to different hydration heat characteristics [24], which can be accurately captured by the adiabatic temperature rise test. This was also the method used in the current study to determine the heat generation rate of the concrete, ensuring the validity and accuracy of the numerical simulations. The results showed that the performed FEA was able to reflect well the temperature variation patterns of the thick raft concrete foundation structures induced by the heat of hydration.

3.2.3. FEA of the Foundations with Different Thicknesses. An FEA was performed on the temperature fields of five foundations with various thicknesses (i.e., 1.65 m, 3.30 m, 4.95 m, 6.60 m, and 9.90 m) but similar material properties and horizontal cross-section size with Foundation 1 to examine the role of foundation thickness in temperature variation. Figure 15 plots the temperature at the concrete core versus time for foundations with different thicknesses. The temperature peak increased with the increase in the raft thickness, but not in a significant manner. The thicker the raft was, the longer the high-temperature (close to the peak temperature) period lasted. For instance, at 18 days after pouring, the core temperature for the 1.65 m thick foundation dropped to 54% of the peak temperature. The core temperature of the 3.30 m thick foundation dropped to 80% of its peak temperature at the same age, and this percentage for 9.90 m was as high as 98%. The reason for this is simple—thinner foundations were fast in heat dissipation, causing the core temperature to rapidly drop. Furthermore, the heat transfer distance in the vertical direction will be longer as the foundation thickness increases, leading to the slow decline of the core temperature.

Figures 16–18 show the temperature difference between the core and the upper surface of the foundations with thicknesses of 1.65 m, 2.50 m, and 9.90 m, respectively. Heat convection existed between the concrete and air because of the impact of the ambient environment surrounding the foundation; hence, regardless of the foundation thickness, the temperature at the upper surface was always close to the ambient temperature. The high-temperature period of a thicker foundation lasted longer, so does the temperature difference between the concrete core and surface, resulting

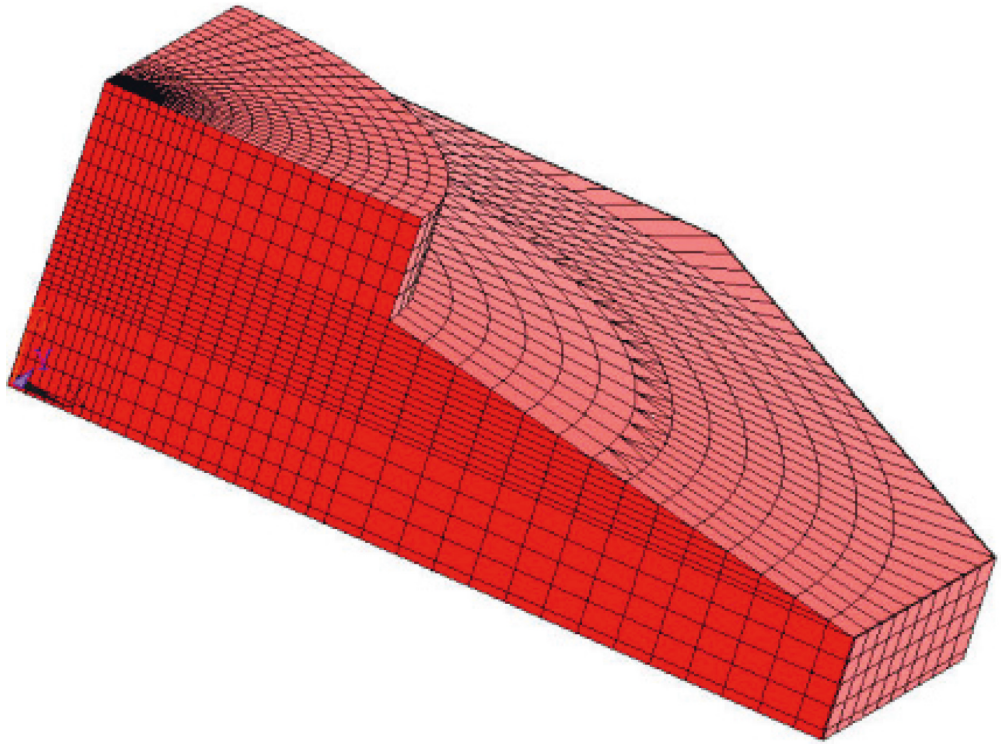

Figure 11: FEA meshing.

Table 2: Main thermal parameters.

Properties	Value adopted in the analysis
Heat conductivity of concrete (kJ/(m·h·°C))	8.0
Specific heat of concrete (kJ/(kg·°C))	0.97
Density of concrete (kg/m^3)	2400
Heat conductivity of soil (kJ/(m·h·°C))	5.0
Specific heat of soil (kJ/(kg·°C))	1.273
Density of soil (kg/m^3)	1800
Concrete-air heat transfer coefficient (kJ/(m^2·h·°C))	100
Steel mold-air heat transfer coefficient (kJ/(m^2·h·°C))	95

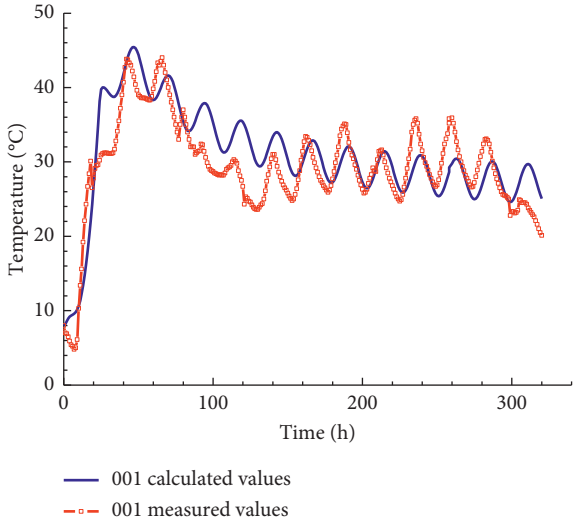

Figure 12: Comparison between the calculated and measured values for Point 001.

in a higher temperature gradient. In other words, the vertical temperature gradient positively depended on the foundation thickness. According to the simulation results, for instance, the maximum temperature difference for the 1.65 m thick foundation was 18°C, whereas that for the 9.90 m thick foundation was 42°C. Sufficient thermal stress would lead to cracking when the temperature difference exceeds a certain value. Therefore, the temperature difference between the concrete core and surface can be considered as a critical indicator for crack risk assessment and crack prevention [25].

As stated earlier, 25°C is a commonly recognized temperature difference threshold, above which temperature control measures need to be taken to avoid thermal cracking. Therefore, the raft thickness corresponding to the 25°C temperature difference should be considered as the thickness threshold requiring temperature control. According to the current analysis (Figure 17), the maximum temperature difference between the concrete core and surface for the 2.50 m thick foundation was 25°C; hence, 2.50 m can be viewed as the thickness threshold, above which effective measures should be taken to reduce the temperature gradient, preventing concrete cracking caused by excessive thermal stress.

4. Temperature Control Measures

Various methods for controlling thermal cracking have been proposed based on the previously reported case studies on

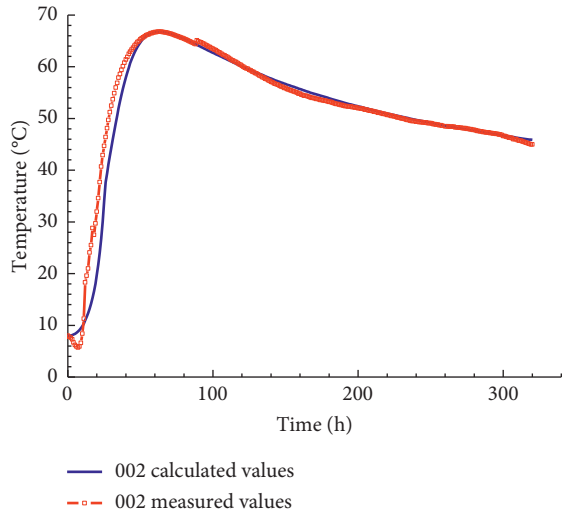

Figure 13: Comparison between the calculated and measured values for Point 002.

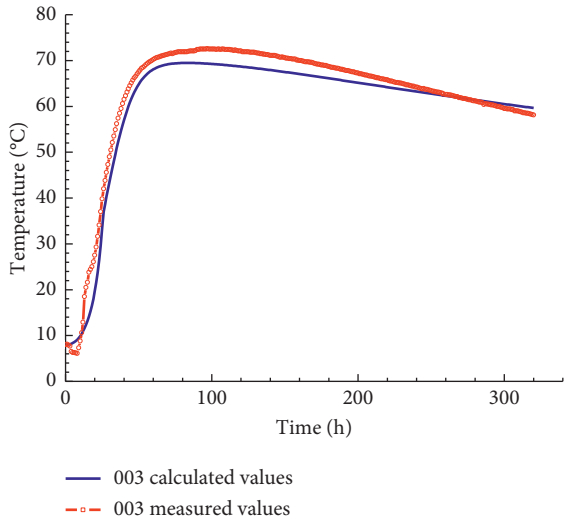

Figure 14: Comparison between the calculated and measured values for Point 003.

cracking of concrete dams [26–28]. The commonly used ones can be grouped into four categories: enhancing the cracking strength of the concrete, lowering heat generation, temperature control, and improving constraints. Based on the temperature test data of Foundation 1 in the present study, the temperature control approach was adopted for foundations 2–21 considering the relatively small volume of wind turbine foundations and other factors, such as field construction difficulties. This approach featured a comprehensive suite of feedback regulation measures, including layered pouring, thermal insulation, and in situ real-time temperature monitoring. Layered pouring involves vertical division of the foundation according to a certain thickness and control of the casting time interval between layers, such that the temperature rise of each layer during the heat accumulation phase is not excessive. A sharp decline of the temperature at the concrete surface caused by the sudden cold wave strike can be mitigated by covering and insulating

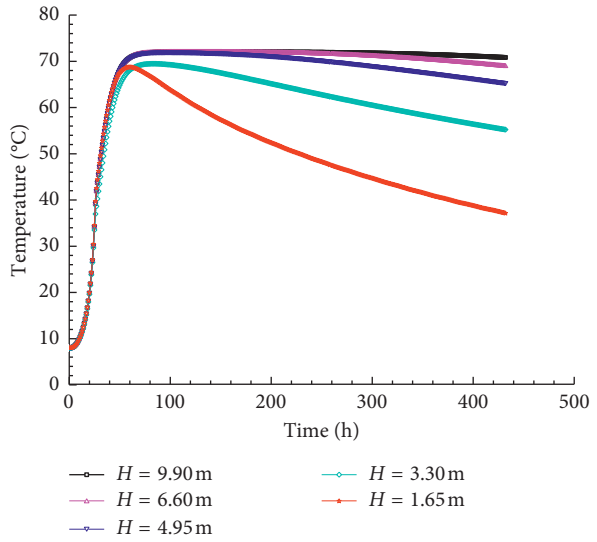

Figure 15: Core temperature evolution of foundations with various raft thicknesses.

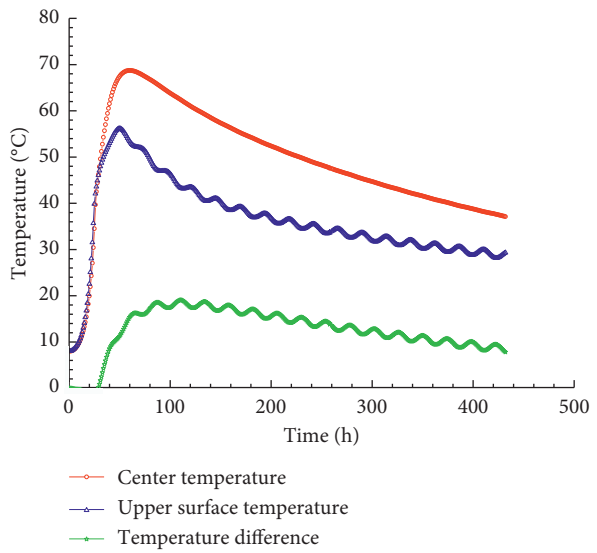

Figure 16: Temperature difference between the core and the upper surface of the 1.65 m thick foundation.

the top surface of the mass concrete structure using traditional insulation materials. In situ real-time temperature monitoring is realized by gathering data from sensors installed at key locations of the representative foundations. Specifically in the current project, (1) the temperature sensors were installed at the core and top surface of foundations 5, 10, 15, and 20; (2) pouring was implemented in three layers, and the time interval between layers was determined based on the real-time measured temperature data; and (3) the foundations were covered with straw-woven insulation materials after the completion of pouring, and the insulation thickness could be adjusted based on weather conditions and real-time measured temperature data.

Through these measures, the temperature differences of the wind turbine foundations were controlled within 25°C.

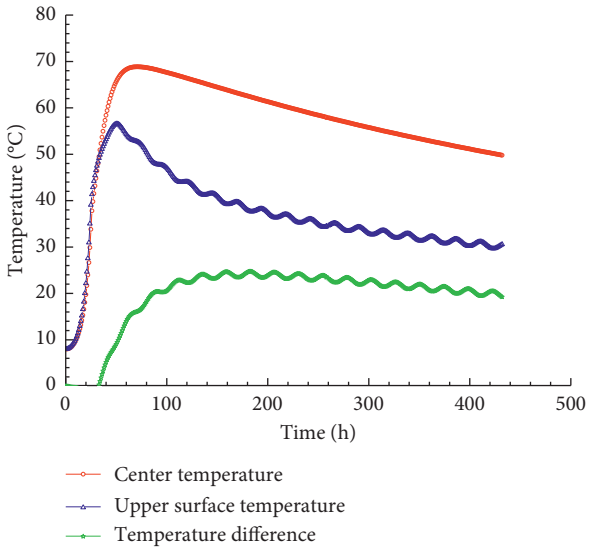

Figure 17: Temperature difference between the core and the upper surface of the 2.5 m thick foundation.

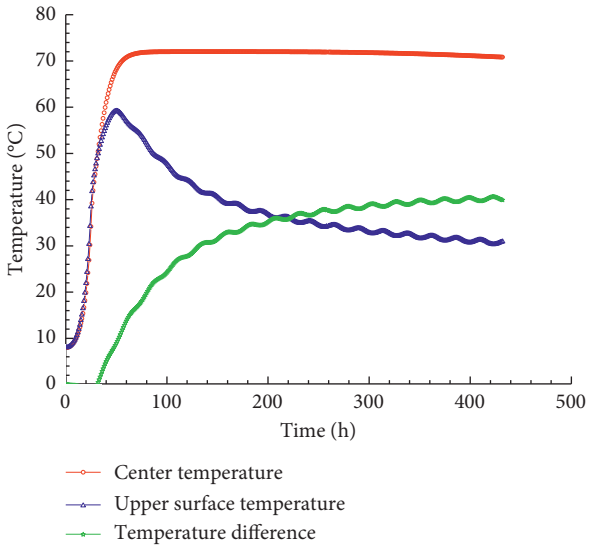

Figure 18: Temperature difference between the core and the upper surface of the 9.9 m thick foundation.

Table 3 presents the temperature measurement results of representative foundations. Figure 19 shows two of the constructed wind turbines and a foundation.

The field test results prove the applicability of the proposed suite of temperature feedback regulation measures, including layered pouring, thermal insulation, and in situ real-time temperature monitoring, to thick raft mass concrete structures with relatively small volumes, thereby achieving good control of the temperature difference between the concrete core and surface, as well as preventing thermal cracking at early ages. Compared to other temperature-based cracking control methods, this approach is simpler and more cost-effective. This approach is expected to be applied more widely with the emergence of novel environmentally friendly insulation materials.

Table 3: Temperature measurement results of representative foundations.

Foundation	Maximum temperature at the foundation core (°C)	Maximum temperature difference between the foundation core and top (°C)
Foundation 5	60.5	20.5
Foundation 10	62.0	22.0
Foundation 15	58.6	18.2
Foundation 20	57.2	18.0

(a)

(b)

Figure 19: Wind turbines and foundation after the completion of construction: (a) two of the constructed wind turbines and (b) a constructed foundation.

5. Conclusions

The following conclusions are obtained in this study:

(1) In situ monitoring showed that the temperature evolution of the concrete foundation at early ages could be categorized into two characteristic phases: heat accumulation and heat release phases. The temperature at the concrete core peaked at 73°C 4 days after pouring, then slowly declined to an approximately steady level.

(2) An evident temperature gradient in the vertical direction of the foundation was observed. The

maximum temperature difference between the concrete core and the top surface at an age of 9 days was as high as 35°C. Such large temperature gradients led to cracking risks.

(3) The concrete heat generation rate used in the temperature-field FEA was based on the adiabatic temperature rise test, ensuring high accuracy of the numerical simulations. The simulated results were in good agreement with the measured data.

(4) The FEA on the temperature fields of foundations with various thicknesses showed that thicker foundations corresponded to higher temperature gradients. Thermal cracking was likely to occur when the raft thickness was larger than 2.50 m, which corresponds to a maximum temperature difference between the concrete core and surface higher than 25°C; hence, temperature control measures should be taken.

(5) The field test results validated the applicability of the proposed suite of temperature feedback regulation measures, including layered pouring, thermal insulation, and in situ real-time temperature monitoring, to thick raft mass concrete structures with relatively small volumes, achieving good control of the temperature difference between the concrete core and the surface, as well as prevention of thermal cracking at early ages. This approach is simpler and more cost-effective compared to other temperature-based cracking control methods.

Data Availability

The data used to support the findings of this study are available from the corresponding author upon request.

Conflicts of Interest

The authors declare that they have no conflicts of interest regarding the publication of this paper.

Acknowledgments

This study was supported by the National Natural Science Foundation of China (no. 51178287) and the Natural Science Foundation of Shanxi Province, China (no. 2011011024-1).

References

[1] C. R. Bobko and V. Z. Zadeh, "Improved schmidt method for predicting temperature development in mass concrete," *ACI Materials Journal*, vol. 112, no. 4, pp. 579–586, 2015.

[2] W. R. L. D. Silva, V. Smilauer, and P. Stemberk, "Upscaling semi-adiabatic measurements for simulating temperature evolution of mass concrete structures," *Materials and Structures*, vol. 48, no. 4, pp. 1031–1041, 2015.

[3] M. H. Lee, B. S. Khil, and H. D. Yun, "Influence of cement type on heat of hydration and temperature rise of the mass concrete," *Indian Journal of Engineering and Materials Sciences*, vol. 21, no. 5, pp. 536–542, 2014.

[4] X. H. Liu, C. B. Zhou, X. L. Chang et al., "Simulation of mass concrete temperature cracking propagation process," *Rock and Soil Mechanics*, vol. 31, no. 8, pp. 2666–2671, 2010.

[5] M. J. Heap, Y. Lavallée, A. Laumann et al., "The influence of thermal-stressing (up to 1000°C) on the physical, mechanical, and chemical properties of siliceous-aggregate, high-strength concrete," *Construction and Building Materials*, vol. 42, no. 5, pp. 248–265, 2013.

[6] J. Conceição, R. Faria, M. Azenha, F. Mamede, and F. Souza, "Early-age behaviour of the concrete surrounding a turbine spiral case: monitoring and thermo-mechanical modelling," *Engineering Structures*, vol. 81, pp. 327–340, 2014.

[7] W. Liu, B. Q. Dong, W. W. Li et al., "The study on thermal stress and temperature crack of underground mass concrete," *Industrial Construction*, vol. 38, no. 7, pp. 79–82, 2008.

[8] R. Faria, M. Azenha, and J. A. Figueiras, "Modelling of concrete at early ages: application to an externally restrained slab," *Cement and Concrete Composites*, vol. 28, no. 6, pp. 572–585, 2006.

[9] B. F. Zhu, *Thermal Stresses and Temperature Control of Mass Concrete*, People's China Water Power Press, Beijing, China, 2012.

[10] S. Sabbagh-Yazdi, T. Amiri-SaadatAbadi, and F. M. Wegian, "2D Linear Galerkin finite volume analysis of thermal stresses during sequential layer settings of mass concrete considering contact interface and variations of material properties Part 2: stress Analysis," *Journal of the South African Institution of Civil Engineering*, vol. 55, no. 1, pp. 104–113, 2013.

[11] K. A. Riding, J. L. Poole, A. K. Schindler et al., "Evaluation of temperature prediction methods for mass concrete members," *ACI Materials Journal*, vol. 103, no. 5, pp. 357–365, 2006.

[12] Y. Li, L. Nie, and B. Wang, "A numerical simulation of the temperature cracking propagation process when pouring mass concrete," *Automation in Construction*, vol. 37, pp. 203–210, 2014.

[13] L. S. Shi, "Formation mechanism and prevention measures of building temperature crack," *China High-Tech Enterprises*, vol. 337, no. 22, pp. 121-122, 2015.

[14] P. Lin, H. Hu, D. Zheng et al., "Field tests on the evolution of a real thermal field in concrete," *Journal of Tsinghua University (Science and Technology)*, vol. 55, no. 1, pp. 27–32, 2015.

[15] Y. N. Hou, *On the Control and Measures to Deal with Crack in Mass Concrete*, Shan Dong University, Ji'nan, China, 2007.

[16] Y. G. Huang, *Thermal Measure and Crack Control of Mass Concrete*, Xi`an University of Architecture and Technology, Xi'an, China, 2004.

[17] Y. Li, C. S. Guan, J. Chen et al., "Numerical simulation on mass concrete floor temperature field and stress field of 117 building," *Concrete*, vol. 274, no. 8, pp. 122–124, 2012.

[18] Y. W. Ju, K. F. Li, and J. G. Han, "Experimental and theoretical research on tensile creep of early-age concrete," *Engineering Mechanics*, vol. 26, no. 9, pp. 43–49, 2009.

[19] N. Qian and Z. J. Xue, "Crack and deficit treatment of dam concrete for Lijiaxi Hydropower Station," *Northwest Water Power*, vol. 4, no. 4, pp. 29–31, 2000.

[20] C.-k. Lim, J.-K. Kim, and T.-S. Seo, "Prediction of concrete adiabatic temperature rise characteristic by semi-adiabatic temperature rise test and FEM analysis," *Construction and Building Materials*, vol. 125, pp. 679–689, 2016.

[21] N. Liu and G. T. Liu, "Random temperature field of mass concrete structure solved by stochastic finite element method," *Journal of Tsinghua University (Science and Technology)*, vol. 36, no. 1, pp. 41–47, 1996.

[22] Y. Yuan, *Crack Control Method to Concrete Structure at Early Ages*, Science Press, Beijing, China, 2003.
[23] Y. W. Ju, K. F. Li, and J. G. Han, "Early-age stress analysis of concrete diaphragm wall through tensile and compressive creep modeling," *Engineering Mechanics*, vol. 26, no. 11, pp. 80–87, 2009.
[24] A. Schackow, C. Effting, I. R. Gomes, I. Z. Patruni, F. Vicenzi, and C. Kramel, "Temperature variation in concrete samples due to cement hydration," *Applied Thermal Engineering*, vol. 103, pp. 1362–1369, 2016.
[25] S. Qiang and M. Z. Liu, "A new safety factor prediction model for mass concrete surface cracking in early age," *Mathematical Problems in Engineering*, vol. 2014, Article ID 183209, 15 pages, 2014.
[26] P. Lin, H. Y. Liu, Q. B. Li et al., "Effects of outlets on cracking risk and integral stability of super-high arch dams," *Scientific World Journal*, vol. 2014, Article ID 312827, 19 pages, 2014.
[27] P. Lin, T. Ma, Z. Liang, C. A. Tang, and R. Wang, "Failure and overall stability analysis on high arch dam based on DFPA code," *Engineering Failure Analysis*, vol. 45, pp. 164–184, 2014.
[28] R. K. Wang, P. Lin, and W. Y. Zhou, "Study on cracking and stability problems of high arch dams on complicated foundations," *Chinese Journal of Rock Mechanics and Engineering*, vol. 26, no. 10, pp. 1951–1958, 2007.